Highly Selective Cu Staining of Sulfur-Containing Polymers Facilitates 3D Nanomorphology Reconstruction of Polymer:Fullerene Blends in Organic Solar Cells by FIB-SEM Tomography

Yonghe Li,* Martin Čalkovský, Erich Müller, Christian Sprau, Alexander Colsmann, and Dagmar Gerthsen*

ABSTRACT: The distinction of different organic materials in phase mixtures is hampered in electron microscopy because electron scattering does not strongly differ in carbon based materials that mainly consist of light elements. A successful strategy for contrast enhancement is selective staining where one phase of a material mixture is labeled by heavier elements, but suitable staining agents are not available for all organic materials. This is also the case for bulk heterojunction (BHJ) absorber layers of organic solar cells, which consist of interpenetrating networks of donor and acceptor domains. The domain structure strongly influences the power conversion efficiency, and nanomorphology optimization often requires real space information on the sizes and interconnectivity of domains with nanometer resolution. In this work, we have developed an efficient approach to selectively stain sulfur containing polymers by homogeneous Cu infiltration, which generates strong material contrast in scanning (transmission) electron microscopy (S(T)EM) images of polymer:fullerene BHJ layers. Cross section lamellae of BHJ layers are prepared for STEM by focused ion beam milling and are attached to a Cu lift out grid as a copper source. After thermal treatment at 200 °C for 3 h in air, sulfur containing polymers are homogeneously infiltrated by Cu, while the fullerenes are not affected. Selective Cu staining is applied to map the phase distribution in PTB7:$PC_{71}BM$ BHJ layers fabricated with different processing additives to tailor the nanomorphology. The strong contrast between polymer and fullerene domains is the prerequisite for the three dimensional reconstruction of the domain structure by focused ion beam/scanning electron microscopy tomography.

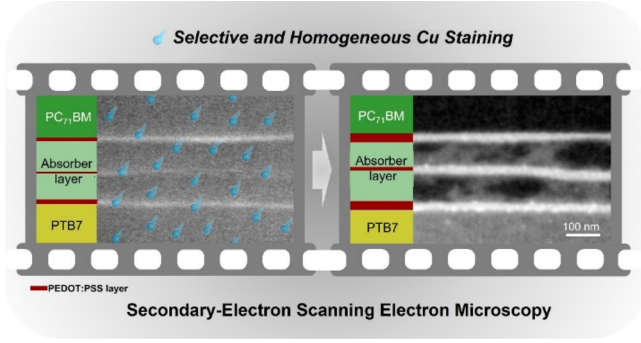

KEYWORDS: *selective Cu staining, conjugated polymer, fullerene, organic solar cell, FIB SEM tomography*

INTRODUCTION

The structural properties of phase mixtures of organic materials are of tremendous relevance in materials and life sciences, for example, to tailor the optoelectronic properties of organic solar cells. If structure information on the nanoscale is needed, electron microscopy is often the method of choice due to its inherent high spatial resolution. However, the distinction of different carbon based materials is often hampered by weak material contrast in scanning electron microscopy (SEM) and (scanning) transmission electron microscopy ((S)TEM) images. This low contrast originates from the similar material properties and, hence, similar electron scattering properties because organic materials mainly consist of light elements such as hydrogen, carbon, oxygen, and nitrogen without additions of heavier elements. Moreover, organic materials often lack long range crystalline structures, eliminating Bragg diffraction contrast as an alternative for contrast generation.

For decades, a successful strategy for the enhancement of material contrast has been selective staining where one phase of a material mixture is labeled by heavier elements. This increases the atomic number difference of the materials and yields an enhanced material contrast. Staining agents like OsO_4/RuO_4 or uranylacetate are commonly used to label organic materials,[1−3] exploiting their interaction with unsaturated/double carbon bonds and carboxyl groups. However, staining can lead to the swelling of nanoscaled phases, and, more seriously, these

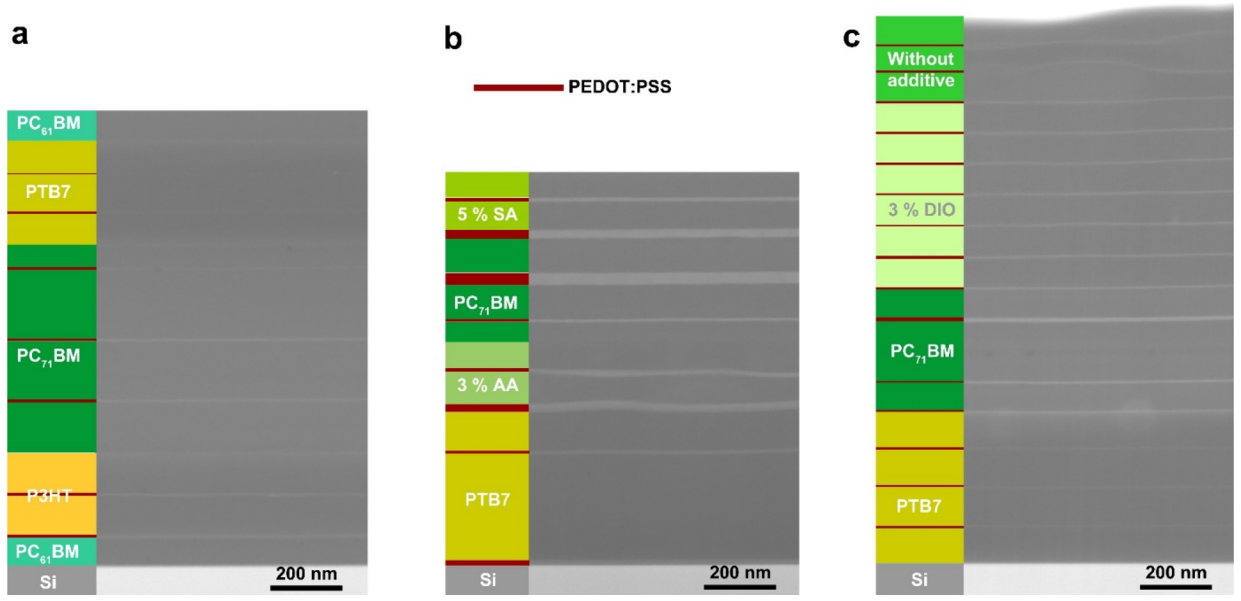

Figure 1. The 200 keV HAADF STEM images of as prepared lamellae from multilayer stacks with corresponding schemes. (a) Stack consisting of pure $PC_{61}BM$/PTB7/$PC_{71}BM$/P3HT/$PC_{61}BM$ layers (*sample pure*). (b, c) Two stacks of pure layers and additive processed BHJ layers with (b) 5% SA processed PTB7:$PC_{71}BM$/pure $PC_{71}BM$/3% AA processed PTB7:$PC_{71}BM$/pure PTB7 and (c) additive free PTB7:$PC_{71}BM$/3% DIO processed PTB7:$PC_{71}BM$/pure $PC_{71}BM$/pure PTB7. The detailed arrangement of the layers consisting in some case of several sublayers of the same type is shown in corresponding schemes. PEDOT:PSS layers between different sublayers (marked by red lines in the schemes) are frequently observed, which are undissolved remnants from the fabrication process of single layers (cf. Materials and Methods).

staining agents are highly toxic. Moreover, suitable staining agents are not available for all organic material systems. This also applies to absorber layers of bulk heterojunction (BHJ) organic solar cells (OSCs), which consist of three dimensional (3D) interpenetrating networks of acceptor and donor domains. Yet, information on the structural properties of the domains (sizes and interconnectivity) is crucially important because the structural properties strongly influence the power conversion efficiency.[4,5] Several electron microscopic techniques have been successfully used for nanomorphology imaging and domain size determination of BHJs, which often contain fullerene derivatives and conjugated polymers. Standard bright field TEM imaging was applied,[6−8] which requires, however, defocusing to achieve phase contrast at the expense of spatial resolution and delocalization of image information. Energy filtering (EF) TEM[7,9−11] and energy filtering SEM[12] are also adequate techniques for phase sensitive imaging. In another approach, STEM at comparably low electron energies was performed, which yields improved contrast due to a higher signal to noise ratio.[13,14] A 4D STEM pair distribution function analysis was carried out to resolve domains in polymer:fullerene blends, but this technique requires laborious data analysis.[15] All techniques mentioned above yield two dimensional (projection) images of the 3D domain structure in BHJs. However, even more desirable is the reconstruction of the 3D structure to allow an improved assessment of the interconnectivity of the domain networks. Not many studies are found so far in the literature where TEM,[16−20] STEM,[19,21,22] or EFTEM tomography[23−25] was applied for the 3D reconstruction of organic BHJs, and these approaches are impeded by the low contrast of the different phases. The selective staining of donor or acceptor phases in polymer: fullerene absorber layers of OSCs could be a viable approach for contrast enhancement, but staining approaches based on selective vaporized metal precursor infiltration of ZnO have only recently emerged.[19−21] This technique allows one to distinguish phase separations on the scale >50 nm, but the visualization of smaller phase segregations <50 nm and domains with sizes below 15 nm is hampered by blurring due to the overlap of contrast induced by the embedded ZnO nano particles.

To overcome these constraints, we describe in this work a new facile procedure for highly selective Cu staining of sulfur containing polymers, which allows one to clearly distinguish polymer and fullerene phases in BHJs. The staining procedure was investigated using model samples that consist of layers of pure conjugated polymers poly(3 hexylthiophen 2,5 diyl) (P3HT, $(C_{10}H_{14}S)_n$) and poly[(4,8 bis[(2 ethylhexyl)oxy] benzo[1,2 b:4,5 b′]dithiophene 2,6 diyl][3 fluoro 2 [(2 ethylhexyl)carbonyl]thieno [3,4 b]thiophenediyl)] (PTB7, $(C_{41}H_{53}FO_4S_4)_n$) as well as the fullerenes [6,6] phenyl C_{71} butric acid methyl ester ($PC_{71}BM$) and [6,6] phenyl C_{61} butyric acid methyl ester ($PC_{61}BM$). These materials are often used in light harvesting BHJs in OSCs. Focused ion beam (FIB) prepared TEM lamellae attached to Cu lift out grids as the copper source were thermally treated at 200 °C for 3 h in air. After thermal treatment, highly selective Cu infiltration of the conjugated polymers (P3HT and PTB7) leads to a strongly enhanced electron scattering, whereas electron scattering and the corresponding STEM intensity of the fullerene phases remain unchanged. The new staining approach was applied to visualize the phase distribution of PTB7:$PC_{71}BM$ BHJ layers processed from neat *o* xylene with different processing additives *m* salicylaldehyde (SA), *p* anisaldehyde (AA), and 1,8 diio dooctance (DIO) that are used to control the domain sizes.[26] Contrast enhancement between polymer and fullerene phases is not only observed in composition sensitive high angle annular dark field (HAADF)STEM images but can be also exploited for secondary electron scanning electron microscopy (SE SEM) imaging. This is the prerequisite for the 3D reconstruction of the domain structure in PTB7:$PC_{71}BM$ BHJ layers by focused ion

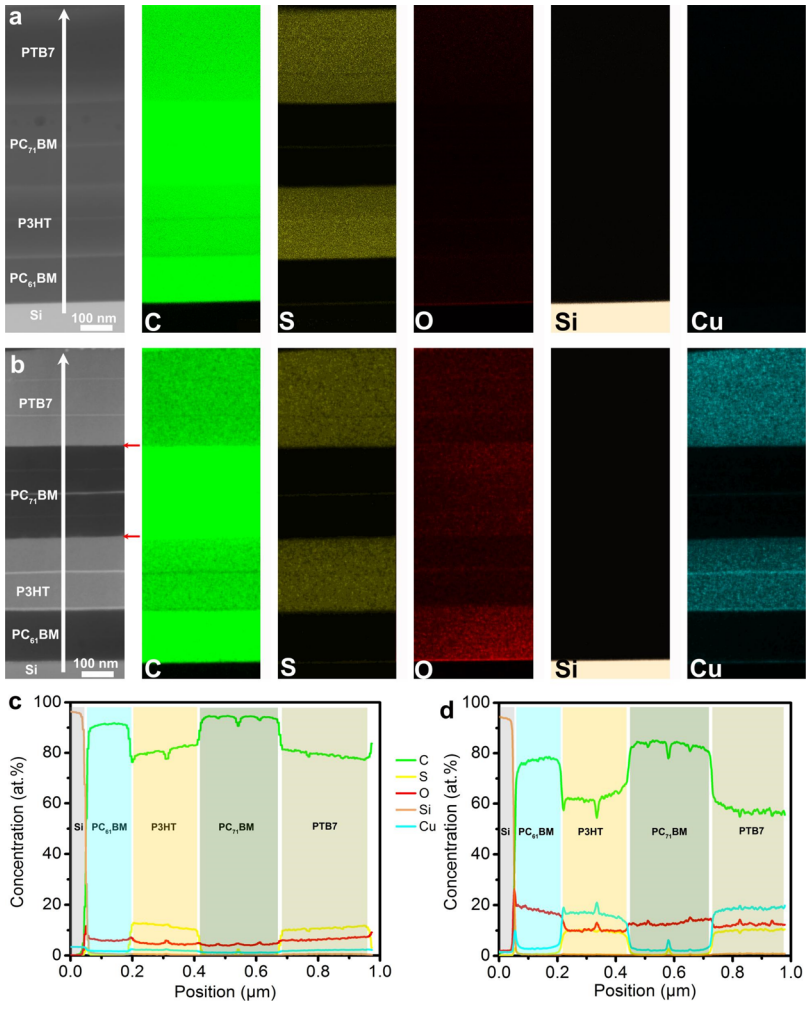

Figure 2. Selective Cu distribution in sulfur containing conjugated polymer layers after thermal treatment at 200 °C for 3 h in air. Comparison of 200 keV HAADF STEM images and C, S, O, Si, and Cu distributions of the PTB7/$PC_{71}BM$/P3HT/$PC_{61}BM$ multilayer stack on Si (*sample pure*) in a TEM lamella with a lamella thickness of about 200 nm (a) before and (b) after thermal treatment and further ion beam milling to a thickness of about 150 nm. The element maps were obtained by energy dispersive X ray spectroscopy (EDXS)/STEM mapping. (c, d) Color coded concentration profiles for the elements C, S, O, Si, and Cu along the white arrows in the HAADF STEM images in panels (a) and (b). The small local concentration maxima and minima within layers result from PEDOT:PSS interlayers between different sublayers.

beam/scanning electron microscopy (FIB SEM) tomography. This is an important addition to the techniques that are available up to now for the 3D reconstruction of BHJ nanomorphologies because larger volumes can be reconstructed than with (S)TEM based techniques. Moreover, FIB SEM tomography of other materials is established in many laboratories worldwide and can also be used in the future for pure organic BHJ based organic solar cells.

RESULTS AND DISCUSSION

Contrast of Conjugated Polymers and Fullerenes. Neat layers of PTB7, P3HT, $PC_{61}BM$, and $PC_{71}BM$ as well as PTB7:$PC_{71}BM$ BHJ layers processed with different additives were prepared and stacked on top of each other (cf. Materials and Methods). Figure 1 shows schemes of three different multilayer stacks and corresponding HAADF STEM images of cross section lamellae prepared by FIB milling. All lamellae were mounted on Cu lift out grids (cf. Materials and Methods). The multilayer stack in Figure 1a contains only pure layers of fullerenes ($PC_{61}BM$ and $PC_{71}BM$) and conjugated polymers (P3HT and PTB7) deposited on a Si substrate and will be denoted as *sample pure*. The P3HT, $PC_{71}BM$, and PTB7 layers consist of two, four, or three thin sublayers of the same type. Thin poly(3,4 ethylenedioxythiophene):polystyrene sulfonate (PEDOT:PSS) interlayers with bright contrast are observed at interfaces between some sublayers in the stack that are remnants from the preparation of the individual sublayers (cf. Materials and Methods). The bright contrast of PEDOT:PSS is induced by a comparatively high S content (cf. S map in Figure 4b), whereas the other layers essentially display the same intensities because their material properties do not differ significantly.

As prepared FIB lamellae of two more layer stacks are shown in Figure 1b,c, which contain PTB7:$PC_{71}BM$ BHJ layers processed with different additives (SA, AA, and DIO) and pure polymer and fullerene layers for reference. The same observations apply as in *sample pure*, namely, only PEDOT:PSS interlayers appear with bright contrast, whereas the intensities of all other layers do not differ significantly. In particular, donor and acceptor domains cannot be distinguished in the BHJ layers. These cross section samples are further discussed in Figures 5 and 6 where analyses of domain sizes and interconnectivity of domains are presented.

We will illustrate the staining procedure by focusing first on the TEM lamella of *sample pure* depicted in Figure 1a. Figure 2 shows 200 keV HAADF STEM images (left side) and elemental C , S , O , Si , and Cu distribution maps before (Figure 2a) and after thermal treatment of the sample at 200 °C for 3 h in air (Figure 2b). The initial lamella thickness of 200 nm was reduced by ion milling to about 150 nm after annealing. The reason for the additional ion milling will be explained later in context with Figure S3. Hardly any intensity difference between the different layers is observed in the HAADF STEM image of *sample pure* before annealing with the exception of the PEDOT:PSS layers at the interfaces (Figure 2a). After thermal treatment, a strong contrast enhancement is found (Figure 2b) with PTB7 and P3HT showing distinctly higher intensities than $PC_{61}BM$ and $PC_{71}BM$. We note that the absolute intensities of the HAADF STEM images in Figure 2a,b cannot be directly compared because the amplification for image acquisition was different. The origin of the contrast enhancement is revealed by the elemental distributions in Figure 2a,b obtained from energy dispersive X ray spectroscopy (EDXS)/STEM mapping. The presence of sulfur in the conjugated polymers correlates with a substantial Cu content after thermal treatment. In contrast, sulfur is not contained in the fullerene layers, which do not show any Cu uptake after thermal treatment. EDXS spectra from the corresponding elemental maps were quantified along lines through the whole layer stack (cf. arrows in the HAADF STEM images in Figure 2a,b). The Cu content after thermal treatment (Figure 2d) reaches values as high as 18% in the polymers, whereas only a small Cu concentration (~2 at. %) is detected in the as prepared lamella (cf. Figure 2c, blue line). The negligible Cu concentration in the as prepared lamella (Figure 2a) shows that the increased Cu content in the thermally treated lamella is not related to stray X rays from the Cu lift out grid. We also observe an increased O concentration that is attributed to oxygen adsorption and reaction with side chains during thermal annealing in air. Apart from different absolute atom concentrations due to the additional Cu and O contents in the annealed lamella, there is no obvious change of the C and S distributions compared to the as prepared state. Obviously, the selective uptake of Cu during thermal treatment increases the average atomic number of conjugated polymers and leads to an increase of the HAADF STEM intensity in these materials. Regarding the S content in the PEDOT:PSS layers (yellow line in Figure 2c,d), we note that the electron beam does not propagate perfectly parallel to the very thin PEDOT:PSS layers. Therefore, EDXS will also contain information from the adjacent layers with a lower S content or without S at all. This effect reduces the measured S concentration compared to the real S content. The latter may also vary because the PEDOT:PSS layers are remnants of the fabrication process and the S content in the layers can be different depending on the degree of dissolution of the PEDOT:PSS after removal from the substrate. Detailed studies of interfaces without PEDOT:PSS interlayers (marked by red arrows in the HAADF STEM image in Figure 2b) show abrupt contrast changes between fullerene and polymer layers indicating that substantial interdiffusion does not take place. This observation differs from previous observations of thermal driven intermixing of bilayers of conjugated polymers and fullerenes.[27−30] We suggest that the lack of interdiffusion is related to the substantial Cu uptake that acts as a structure fixation as observed for other staining agents.[35]

A structural characterization of *sample pure* with a higher resolution was performed after thermal treatment to obtain more detailed information on the polymer/fullerene interfaces and structural features related to the infiltrated Cu (Figure 3 and

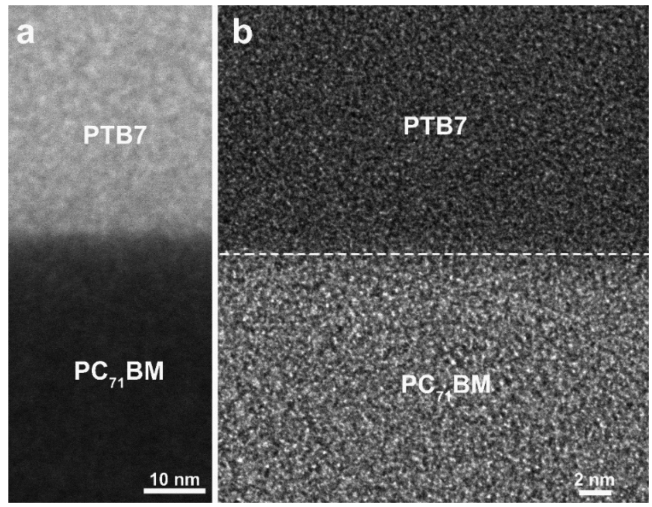

Figure 3. Structural properties of $PC_{71}BM$ and Cu containing PTB7 layers of *sample pure* after thermal treatment. (a) The 200 keV high magnification HAADF STEM image of a region containing $PC_{71}BM$ and PTB7 layers and (b) the corresponding high resolution (HR)TEM image.

Figure S1). The high magnification HAADF STEM image of the PTB7/$PC_{71}BM$ interface region of *sample pure* (Figure 3a) shows a strong contrast between PTB7 and $PC_{71}BM$ and a rather abrupt interface between the two materials. High resolution (HR)TEM imaging (Figure 3b) demonstrates the absence of clusters and crystalline structures in PTB7 and indicates that Cu is homogeneously distributed in PTB7. We note that the contrast of $PC_{71}BM$ and PTB7 is inverted with respect to the HAADF STEM image due to the bright field nature of HRTEM images. STEM and HRTEM images of the P3HT/$PC_{61}BM$ interface in *sample pure* (Figure S1) confirm the observations in Figure 3, *i.e.,* a distinct contrast between polymer and fullerene layers after thermal treatment (Figure S1a) and the absence of crystalline structures due to Cu in the polymer (Figure S1b). We thus conclude that Cu is present in the atomic solution in the conjugated polymers PTB7 and P3HT after thermal treatment, although the Cu content is rather high.

Proposed Mechanism of Contrast Generation. To clarify the origin of selective Cu uptake in the P3HT and PTB7 polymers, the structural and chemical features of *sample pure* were investigated before reducing the TEM lamella thickness after thermal treatment. SEM imaging shows that the lamella surface is completely covered by high density nano scaled islands (Figure S2). The selected area electron diffraction (SAED) pattern in Figure S2c of the entire layer stack shows sharp rings, which must originate from the nanoislands on the lamella surface because the layers in *sample pure* do not contain any crystalline structures before and after thermal treatment (Figure S3 and Figure 3b). The analysis shows that the islands consist of Cu_2O with a cubic structure ($Pn3m$, a = 4.27 Å, JCPDS file no. 05 0667). An explanation for the Cu infiltration of the sulfur containing polymers is provided by previous reports according to which Cu preferably reacts with S during the interfacial interaction of a P3HT/Cu film.[31,32] However, it is unlikely that the Cu_2O islands act as a copper source because

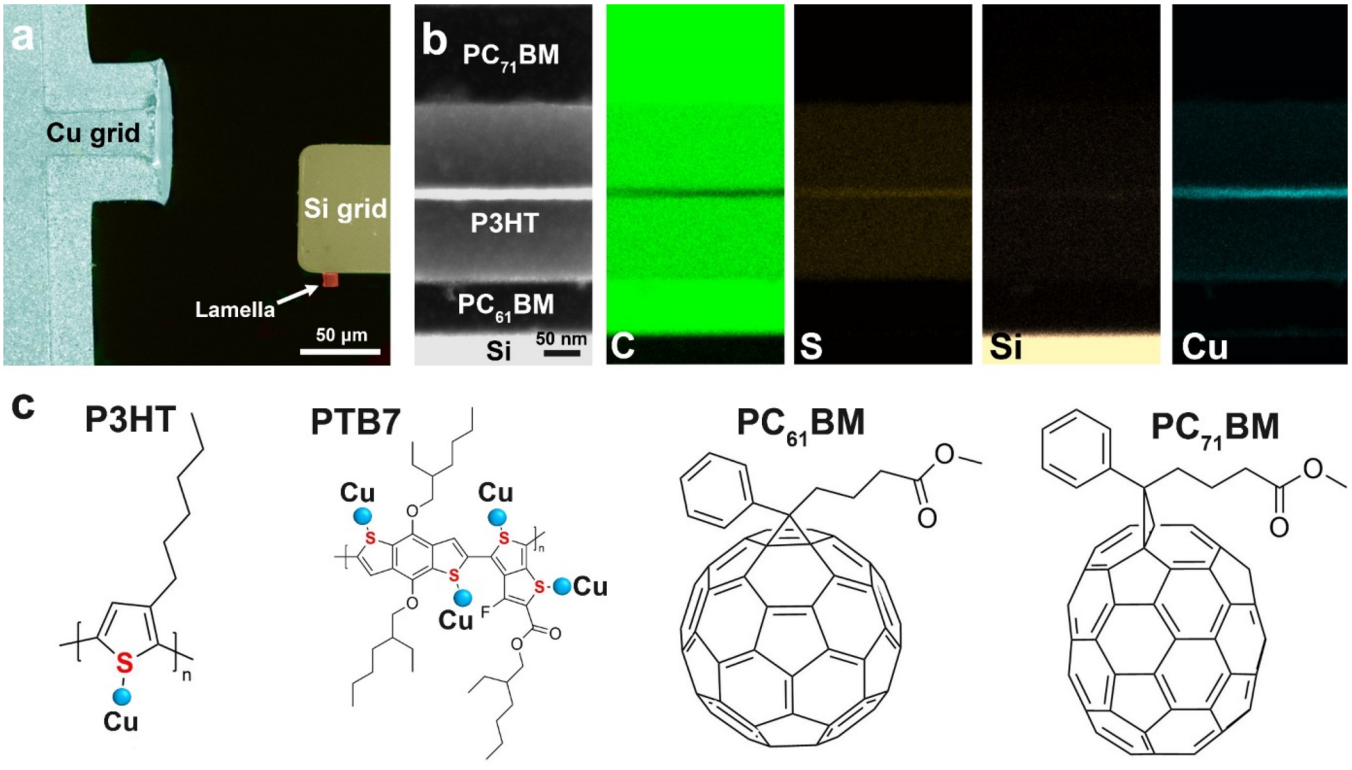

Figure 4. Origin of the selective Cu distribution in conjugated polymers after thermal treatment in air at 200 °C for 3 h. (a) Experimental configuration of a cross section lamella of *sample pure* attached to a Si lift out grid that is placed in the vicinity of a Cu lift out grid as a Cu source for thermal treatment. (b) The 200 keV HAADF STEM cross section image and element maps of C, S, Si, and Cu obtained by STEM EDXS mapping and (c) the proposed formation of Cu−S coordination in P3HT and PTB7.

Cu_2O is a stable phase and it is, hence, unlikely that Cu is released from the islands into the polymer layers. Nevertheless, island formation requires the removal of the islands by FIB milling after thermal treatment because the island contrast interferes with the contrast of the layers.

To clarify the preferential Cu diffusion into the polymers, an additional experiment was performed as shown in Figure 4a. A lamella of *sample pure* was attached to a Si lift out grid, and a Cu lift out grid was placed in a short distance as the copper source. After the same thermal treatment, we observe a significant material contrast enhancement in HAADF STEM images and selective Cu uptake in P3HT in corresponding element maps (Figure 4b). These observations clearly suggest that Cu transport is a gas phase process from the neighboring Cu grid. Compared to the lamella mounted on a Cu grid (Figure S3a,b), dense Cu_2O nanocrystals are not observed on the lamella surface. This finding can be attributed to the smaller amount of copper that is transported to the lamella due to the larger distance from the Cu source. A homogeneous Cu distribution will result if the Cu atoms are coordinated with S sites (cf. Figure 4c), which is a plausible explanation for the uniform Cu distribution. This interpretation is strengthened by the HAADF STEM intensity of the thin PEDOT:PSS interlayers in the layer stacks, which exceeds the intensity of P3HT and PTB7 (Figures 2b and 4b) due to the enhanced S and Cu content of PEDOT:PSS (cf. S and Cu maps in Figure 4b). In contrast, suitable Cu bonding sites are not available at fullerene molecules (cf. Figure 4c), explaining the absence of Cu in the fullerene layers. To summarize, Cu is transported from the Cu source to the TEM lamella by a gas phase process during thermal annealing and selectively infiltrates S containing conjugated polymers. This process is exploited to enhance the intensity of scattered electrons in electron microscopy images of these materials and can thus act as an efficient and nontoxic staining agent.

3D Nanomorphology of PTB7:$PC_{71}BM$ Layers. We will demonstrate in the following that selective Cu infiltration can be applied as a convenient staining method to analyze the size and interconnectivity of PTB7 and $PC_{71}BM$ domains in BHJ layers. For this purpose, we analyzed different PTB7:$PC_{71}BM$ layers with nanomorphologies that were tuned by using different processing additives (AA, SA, and DIO) during layer deposition.[26] It will be shown that Cu staining can be exploited not only for STEM imaging but also for SE SEM imaging as a prerequisite for the 3D reconstruction of the BHJ domain structure by FIB SEM tomography. We emphasize that cross section SE SEM images of the domain structure in BHJ are of particular interest because the vertical electron and hole transport paths toward the electrodes in solar cells strongly influence the performance of OSCs.

Figure 5 presents 2 keV cross section SE SEM images of selected regions of the multilayer stacks in Figure 1b,c showing pristine and Cu stained PTB7:$PC_{71}BM$ BHJ layers processed from neat *o* xylene without an additive (Figure 5a), with 3% AA (Figure 5b), with 5% SA (Figure 5c), and with 3% DIO (Figure 5d). The images were acquired from FIB milled cross section lamellae with a thickness of about 2 μm attached to Cu lift out grids. The uppermost images in Figure 5a−d show SE SEM images of the pristine layers (*i.e.,* before Cu staining) where PTB7 and $PC_{71}BM$ domains can be hardly distinguished. In analogy to HAADF STEM images, a strong contrast enhancement is observed by Cu staining of PTB7 after thermal treatment

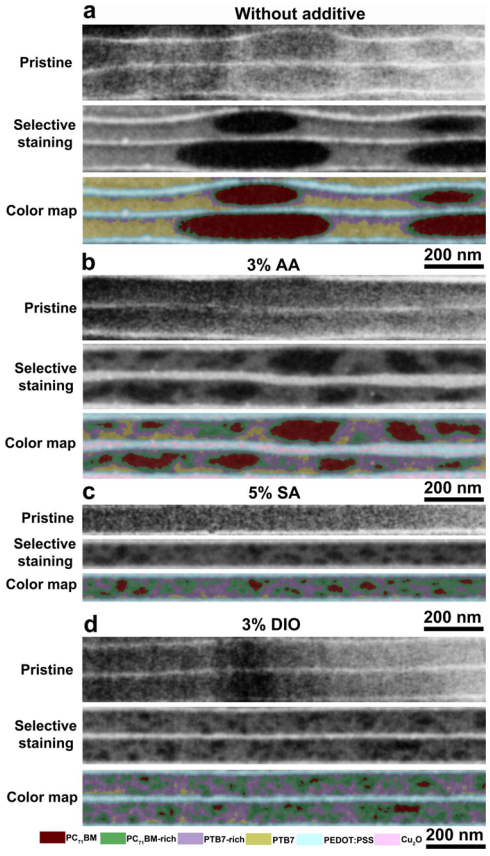

Figure 5. Application of selective Cu staining to enhance PTB7 contrast in PTB7:$PC_{71}BM$ BHJ layers as commonly employed in organic solar cells fabricated with different processing additives. The 2 keV SE SEM cross section images of stacked PTB7:$PC_{71}BM$ layers processed from *o* xylene (a) without additive and with (b) 3% AA, (c) 5% SA, and (d) 3% DIO additives, respectively. Panels (a), (b), and (d) show double layer stacks. The top images were acquired before and the images in the middle were acquired after Cu staining. The bottom images present color coded maps of the phase distribution after phase segmentation using the WEKA algorithm implemented in the Fiji software.[34] The phase assignments were made on the basis of the contrast of pure $PC_{71}BM$ and PTB7 layers contained in the multilayer stacks shown in Figure S4.

at 200 °C for 3 h in air and FIB milling to remove the Cu_2O nanoislands (middle images in Figure 5a–d). We note that SE SEM images are surface sensitive because the exit depth of secondary electrons is only a few nanometers.[33] Therefore, SE SEM images predominantly visualize surface topography. However, FIB milling produces flat surfaces and material contrast can be obtained by SE SEM imaging under such conditions. The enhancement of the SE intensity in Cu stained PTB7 is partly attributed to the increased number of SEs that is generated by backscattered electrons close to the sample surface. Accordingly, the SE intensity of PTB7 domains is strongly enhanced. Pure PT PTB7 and $PC_{71}BM$ layers in the layer stack serve as intensity reference and confirm the phase assignment (cf. Figure S4) with the expected dark contrast for pure $PC_{71}BM$ and bright contrast for pure PTB7. The Cu stained materials show sufficient contrast compared to the fullerene layers to facilitate the segmentation of the SE SEM images into donor (polymer) and acceptor (fullerene) phases. For this purpose, the machine learning based WEKA algorithm implemented in the Fiji software was used.[34] The bottom images in Figure 5a–d present the phase distribution after phase segmentation using the intensities of pure $PC_{71}BM$ and PTB7 layers in the same stack as a reference (Figure S4). We can clearly distinguish $PC_{71}BM$ (marked in dark red) and PTB7 (marked in yellow). In addition, mixtures of PTB7 and $PC_{71}BM$ are observed with intermediate intensities that are classified into $PC_{71}BM$ rich (marked in green) and PTB7 rich (marked in purple), respectively.

The PTB7:$PC_{71}BM$ blend prepared without an additive (Figure 5a) is characterized by isolated and lens shaped pure $PC_{71}BM$ domains with dark contrast and sizes between 200 and 500 nm embedded in the PTB7 matrix. The layer thickness varies and is increased at the position of large $PC_{71}BM$ islands. $PC_{71}BM$ rich regions (marked green in the color coded map in Figure 5a) surrounding the pure $PC_{71}BM$ domains most likely result from projection effects of the spherical domains (cf. plan view image in Figure S5a). The matrix mainly consists of pure PTB7 except for small PTB7 rich regions (marked in purple in the color coded map in Figure 5a) that may be related to the minor $PC_{71}BM$ dissolution in PTB7. However, the BHJ layer fabricated without additives is essentially decomposed into two pure phases ($PC_{71}BM$ and PTB7).

With the addition of 3% AA to the *o* xylene solution (Figure 5b), irregular shaped $PC_{71}BM$ domains with reduced sizes of about 100–200 nm are formed and only a small fraction of pure PTB7 domains preferentially at the bottom of the layers is observed. Compared to the additive free layer, the fraction of PTB7/$PC_{71}BM$ mixtures increases with PTB7 rich and $PC_{71}BM$ rich domains, while pure PTB7 and $PC_{71}BM$ regions are still observed albeit with a smaller size. With the addition of 5% SA during layer deposition (Figure 5c), the size of the $PC_{71}BM$ domains decreases to about 20–50 nm and pure PTB7 domains are rarely observed. Mixtures of PTB7 and $PC_{71}BM$ dominate in this layer and form small scale interconnected PTB7 rich and $PC_{71}BM$ rich regions with sizes below 150 nm. A similar nanomorphology is observed in the PTB7:$PC_{71}BM$ blend that was processed using 3% DIO (Figure 5d). The phase distribution is dominated by a small scale phase separation forming PTB7 rich and $PC_{71}BM$ rich regions with only a few small pure PTB7 and $PC_{71}BM$ domains. The Cu stained PEDOT:PSS interlayers between BHJ layers show even brighter contrast than pure PTB7 and are marked in light blue in the color coded phase distributions. Bright spots are occasionally observed after Cu staining (cf. middle images in Figure 5a,b) that are attributed to remnant Cu_2O islands (bright pink in the color coded maps in Figure 5a,b) that were not completely removed by FIB milling. With respect to the resolution of Cu staining, we note that fullerene and S containing polymer domains with sizes distinctly below 50 nm can be well distinguished. The resolution is clearly improved compared to ZnO staining[19−21] because Cu is present in the atomic solution without the formation of precipitates (cf. Figure 3 and Figure S1).

We note that pure fullerene domains with sizes distinctly below the absorber layer thickness were up to now rarely reported in microscopy studies because they are embedded in a polymer matrix and only mixtures of polymers and fullerenes are visible in plan view images where electrons propagate through BHJ layers from top to bottom in a perpendicular direction. Pure $PC_{71}BM$ domains with small sizes could be revealed in this work in cross section SE SEM images as a direct benefit of selective Cu staining and the multilayer stack architecture. For comparison with the cross section SE SEM images, plan view

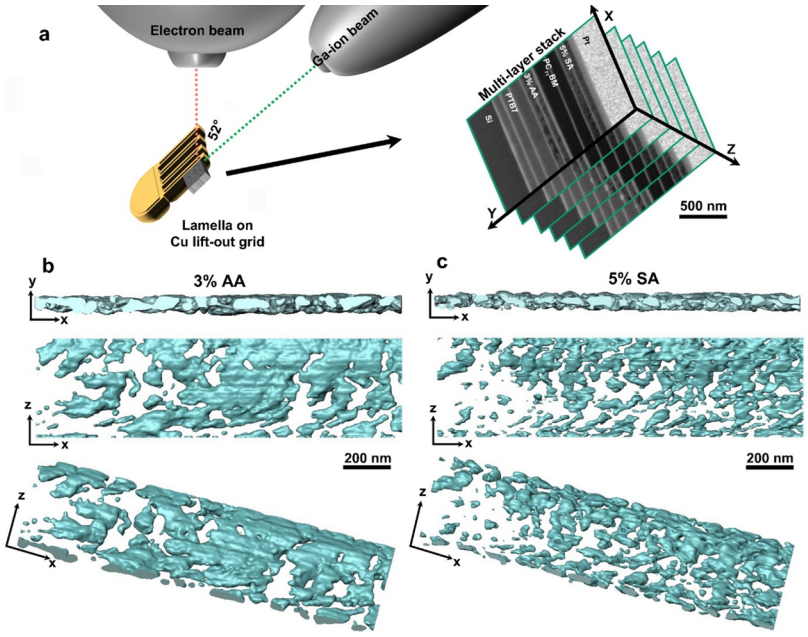

Figure 6. 3D reconstruction of the $PC_{71}BM$ domain structure in PTB7:$PC_{71}BM$ BHJ layers obtained by FIB SEM tomography. (a) Scheme of the experimental setup for FIB SEM tomography and scheme of analyzed multilayer stack containing PTB7:$PC_{71}BM$ processed with 3% AA and 5% SA (cf. Figure 1b). Pure $PC_{71}BM$ and PTB7 layers in the stack act as reference for phase assignment in the blend layers. 3D rendered reconstruction of the pure $PC_{71}BM$ domain structure in PTB7:$PC_{71}BM$ layers processed with (b) 3% AA and (c) 5% SA, respectively. Pure $PC_{71}BM$ domains are displayed in light blue, while mixtures and pure PTB7 regions are transparent. Reconstructions are presented along different viewing directions.

HAADF STEM images of all layers are shown in Figure S5a–d. These layers have not undergone any thermal treatment and show domain sizes and shapes that are well compatible with the phase distribution in the corresponding cross section SE SEM images (Figure 5a–d). They also demonstrate that the obvious coarsening of the domain structure and phase decomposition do not occur during thermal treatment required for staining. We have in addition included plan view images of PTB7:$PC_{71}BM$ layers processed with 3% AA and 5% SA in Figure S6 for comparison between pristine and thermally treated layers at exactly the same position. These images verify that the domain structure is not significantly altered by the heat treatment and Cu may indeed act as a fixation of the original structure because the chemical bonding between Cu and S in polymers prevents interdiffusion between polymers and fullerenes (cf. Figure 2b).

In contrast to 2D images, 3D reconstructions of the domain structure of BHJ layers yield more detailed information on the domain sizes and domain interconnectivity. Up to now, only conventional TEM, HAADF STEM, and EFTEM tomography was performed for the 3D characterization of BHJ blends of OSCs accompanied with the challenges of low contrast and small analyzed volumes.[17,21,23] The strong contrast obtained by selective Cu staining now enables 3D reconstructions of PTB7:$PC_{71}BM$ blends using FIB SEM tomography. An additional benefit results from multilayer stack configurations (cf. images of multilayer stack in Figure 6a) that allow one to efficiently perform 3D reconstructions of several absorber layers within one experiment. We emphasize that 3D reconstruction is only feasible because Cu is present in the atomic solution and does not lead to the formation of clusters or crystallites that may interfere with the contrast of the stained material.

As prototype specimens, we choose the PTB7:$PC_{71}BM$ layers processed with 3% AA (Figure 6b) and 5% SA (Figure 6c) additives. For 3D reconstruction, a lamella with sufficient thickness was prepared from the bulk multilayer stack. The lamella was attached to a Cu lift out grid followed by thermal treatment at 200 °C for 3 h for selective Cu staining. FIB SEM tomography was performed by alternating FIB milling and SE SEM imaging, leading to a stack of 93 images for a reconstructed volume with a thickness of 0.47 μm. The distance between adjacent images was 5 nm. Details on the phase segmentation and reconstruction procedures are given in the methods section (cf. Supporting Information). The blue color in the reconstructions in Figure 6b,c represents the pure $PC_{71}BM$ phase, while mixtures and pure PTB7 regions are transparent. The power conversion efficiency of OSCs is influenced by the domain sizes and domain interconnectivity. Small domains (50–100 nm), as observed in the blend processed with 5% SA (Figure 6c and Movie S2), result in a large interface between donor and acceptor domains and, hence, the efficient separation of electron/hole pairs. On the other hand, domains in this sample are not always well connected, which inhibit charge transport toward the electrodes. The BHJ layer processed with 3% AA shows a different nanomorphology with larger domains (100–500 nm) and good domain interconnectivity (Figure 6b and Movie S1). 3D reconstruction by FIB SEM will facilitate in the future more detailed correlations between photoconversion efficiency and nanomorphology. It is advantageous that the SE SEM imaging of Cu stained S containing polymers is sensitive enough to distinguish between pure compounds (here $PC_{71}BM$ and PTB7) and phase mixtures. Moreover, the surface sensitivity of SE SEM imaging minimizes averaging effects, which cannot be avoided for (S)TEM based techniques, where electrons are affected by structural and chemical inhomogeneities along their path through the sample.

CONCLUSIONS

In this work, a procedure for thermal driven highly selective Cu staining of sulfur containing polymers was developed that leads to a strongly enhanced electron scattering in (S)TEM and SEM

imaging. Staining is the prerequisite for FIB SEM tomography for the 3D reconstruction of bulk heterojunctions in organic solar cells consisting of pure organic compounds and the reconstruction of sample volumes that are significantly larger than for (S)TEM based techniques.

We propose that Cu is coordinated to S sites yielding a homogeneous Cu solution in the conjugated polymers without forming artifacts like Cu clusters or crystallites. This enables imaging of nanoscaled domains with high contrast in polymer: fullerene blends of bulk heterojunction absorber layers of organic solar cells. The required thermal treatment for Cu infiltration does not lead to an obvious modification of the domain structure in polymere:fullerene blends. Using PTB7:$PC_{71}BM$ blends processed from *o* xylene mixed with different additives as a model system, multi length scale phase separation can be analyzed and phases can be segmented into pure $PC_{71}BM$ and PTB7 as well as mixtures of $PC_{71}BM$ and PTB7. This enables the 3D reconstruction of the domain structure of polymer:fullerene blends by FIB SEM tomography. The newly discovered selective Cu staining not only has tremendous merits in (S)TEM and SEM based phase identification in polymer:fullerene systems but is also expected to be a promising approach for the visualization of polymers in other mixtures of organic materials. It furthermore opens a potential road for exploring other metals as nontoxic and efficient staining agents for phase mixtures in block copolymers or other OSC candidates. In addition, homogeneous solutions of Cu or other metals could even be used to tune the electronic and optical properties of organic semiconductors.

MATERIALS AND METHODS

Fabrication of Pure P3HT, PTB7, $PC_{61}BM$, $PC_{71}BM$ Layers, and PTB7:$PC_{71}BM$ Bulk-Heterojunction Layers. All layers were deposited on glass substrates covered by a solution deposited sacrificial layer of poly(3,4 ethylenedioxythiophene):polystyrene sulfonate (PEDOT:PSS, $C_{14}H_{14}O_5S_2$, Clevios VPAI 4083, Heraeus). PEDOT:PSS is water soluble and allows the easy detachment of the layers in water. Pure P3HT, PTB7, $PC_{61}BM$, and $PC_{71}BM$ layers with a thickness of about 90 and 300 nm were prepared as a reference for electron microscopy investigations. Pure P3HT (4002 EE, M_w = 50−70 kg mol^{-1}, regioregularity ≥90%), PTB7 (1 Material Inc., M_w = 131 kg mol^{-1}, $Đ_M$ = 2.5), $PC_{61}BM$ (Solenne, 99%), and $PC_{71}BM$ (Solenne, 99%) were dissolved in *o* xylene (concentration 25 mg mL^{-1}, Sigma Aldrich, anhydrous, 97%) at 85 °C overnight. The corresponding pure material was spin cast (1500 rpm, 60 s, layer thickness 90 nm; 500 rpm, 60 s, layer thickness 300 nm) from a warm (85 °C) solution onto the PEDOT:PSS coated glass substrates and dried at room temperature. PTB7:$PC_{71}BM$ BHJ layers were prepared accordingly. PTB7 and $PC_{71}BM$ were dissolved in *o* xylene (*w*/*w* = 1:1.5, total concentration 25 mg mL^{-1}). Then, *m* salicylaldehyde (SA, Acros Organics, 99%), *p* anisaldehyde (AA, Sigma Aldrich, 98%), or 1,8 diiodooctane (DIO, Alfa Aesar, stabilized with copper, 98%) was added in relation to the main solvent volume (*e.g.,* 1 mL of the main solvent plus 30 μL of the additive is denoted as an additive concentration of 3%). The absorber layers were spin cast (1500 rpm, 60 s, layer thickness 90 nm) from a warm (85 °C) solution onto the substrates and dried at room temperature. Only upon using DIO, an additional drying step was applied at an elevated temperature (50 °C, 20 min) on the next day to remove DIO residues. More details on the absorber layer fabrication are described in the literature.[26]

Fabrication of Multilayer Stacks, TEM-Lamella Preparation, and Selective Cu Staining. For test purposes, a $PC_{61}BM$/PTB7/$PC_{71}BM$/P3HT/$PC_{61}BM$ multilayer stack of pure layers was prepared on a Si substrate by the following procedure. First, pure $PC_{61}BM$, P3HT, $PC_{71}BM$, and PTB7 layers were deposited onto PEDOT:PSS coated glass substrates and were then cut into small pieces with a scalpel. As PEDOT:PSS is water soluble, the layer pieces were floated off the substrate by a drop of water and deposited on top of each other to form a $PC_{61}BM$/PTB7/$PC_{71}BM$/P3HT/$PC_{61}BM$ multilayer stack of pure layers (main manuscript, Figure 1a, *sample pure*). The same procedure was applied to prepare two more multilayer stacks that contain PTB7:$PC_{71}BM$ BHJ layers fabricated without and with different processing additives and pure layers for reference (main manuscript, Figure 1b,c). Since PEDOT:PSS was often not completely dissolved, thin residual interlayers of PEDOT:PSS prevail between different sublayers in the stacks. PEDOT:PSS layers show up with high intensity in high angle annular dark field scanning transmission electron microscopy (HAADF STEM) and secondary electron scanning electron microscopy (SE SEM) images due to their comparably high S and O contents.

Electron transparent STEM lamellae were prepared by Ga focused ion beam (FIB) milling in a Helios G4 FX dual beam instrument (Thermo Fisher Scientific, USA). A Pt protection layer was deposited before FIB milling by electron and ion beam induced Pt deposition. A 30 keV Ga ion beam was used to prepare lamellae with a thickness of about 200 nm for (S)TEM imaging and 2 μm for focused ion beam scanning electron microscopy (FIB SEM) tomography. The lamellae were lifted out from the bulk sample and attached to a Cu lift out grid (Pelco 10GC04, Plano GmbH) or a Si lift out grid (Pelco 21490 10, Plano GmbH) by Pt deposition. Further milling and surface polishing were performed with a reduced ion current of 0.26 nA at 30 keV and in the final stage with 12 pA at 5 keV.

Selective Cu infiltration of FIB prepared lamellae attached to Cu lift out grids was obtained by thermal treatment at 200 °C for 3 h in an oven in ambient air. Thermal treatments were also performed at 200 °C for only 30 and 90 min, which were insufficient for the complete Cu infiltration of lamellae with a thickness of 2 μm that were used for FIB SEM tomography. However, it may be possible to reduce the duration and temperature of the heat treatment if thinner lamellae are investigated. For investigation of the staining mechanism, an FIB prepared lamella attached to a Si lift out grid was thermally treated near a Cu grid as a Cu source under the same annealing conditions.

Electron Microscopy Characterization. Sample preparation by FIB milling and SEM imaging was performed in a Helios G4 FX dual beam microscope (Thermo Fisher Scientific, USA) equipped with a field emission electron gun. SE SEM images of the phase distribution of PTB7:$PC_{71}BM$ BHJ layers were acquired with the through lens detector (TLD) in the immersion mode (2 keV, 0.1 nA). A Tecnai Osiris microscope (Thermo Fisher Scientific, USA) with ChemiSTEM capabilities operated at 200 keV was used to obtain high resolution TEM and HAADF STEM images. Element distribution maps were acquired by energy dispersive X ray spectroscopy (EDXS) STEM using the Super X system of the Tecnai Osiris, which consists of four silicon drift detectors. The EDXS data were recorded and quantified by the Bruker Esprit software. Quantification was carried out by the Cliff−Lorimer method.[36]

FIB-SEM Tomography. For FIB SEM tomography, a lamella with a large thickness of 2 μm was prepared by FIB milling from the layer stacks containing PTB7:$PC_{71}BM$ BHJ layers processed with different processing additives (main paper, Figure 1b,c). A fresh cross section surface was milled by a focused Ga ion beam (30 keV, 0.26 nA) for contrast and brightness optimization. An area of interest (AOI) was selected that was marked by an X shaped fiducial marker on the top of the lamella to correct for sample drift during subsequent serial FIB milling and imaging. Alternating FIB milling and SEM imaging was controlled by the Auto Slice and View 4.0 software with automated focus and sample drift correction. The slice thickness was set to 5 nm, yielding image series consisting of 93 images. FIB milling was performed with an ion beam energy of 30 keV and a low beam current of 0.26 nA. SE SEM images of the newly exposed cross section surfaces were taken with the TLD in the immersion mode (2 keV, 0.1 nA) with a pixel size of 1.25 nm pixel^{-1}. No noticeable mass loss or radiation damage was observed during data acquisition because the contrast between stained polymer and fullerene domains did not change. The built in "Geometric Transformation" function was used to automatically correct the SEM images to compensate for the 52° angle between

the electron and ion beams. After image processing by contrast enhancement and 2 pixel Gaussian blurring, the segmentation of single SE SEM images was performed by the machine learning based WEKA algorithm implemented in the Fiji Software.[34]

Segmentation and 3D surface rendering of the FIB SEM data stack were performed with the Avizo software. The SEM images were first aligned using the least square alignment mode in the Align slices function. In the second step, noise in the aligned SEM images was reduced with the Gaussian filter where the *X* and *Y* standard deviations were set to the value of 4. The segmentation of the processed data stack was performed using a global threshold, where the threshold value was obtained from the reference (pure) $PC_{71}BM$ layer present in the studied multilayer system. In the 3D surface rendering of the segmented data, additional smoothing was applied.

AUTHOR INFORMATION

Corresponding Authors

Yonghe Li − *Laboratory for Electron Microscopy, Karlsruhe Institute of Technology (KIT), Karlsruhe 76131, Germany; Material Research Center for Energy Systems (MZE), Karlsruhe Institute of Technology (KIT), Karlsruhe 76131, Germany;* orcid.org/0000 0001 9552 6088; Email: yonghe.li2@kit.edu, yongheli2016@126.com

Dagmar Gerthsen − *Laboratory for Electron Microscopy and 3DMM2O Cluster of Excellence (EXC 2082/1−390761711), Karlsruhe Institute of Technology (KIT), Karlsruhe 76131, Germany; Material Research Center for Energy Systems (MZE), Karlsruhe Institute of Technology (KIT), Karlsruhe 76131, Germany*; Email: dagmar.gerthsen@kit.edu

Authors

Martin Čalkovský − *Laboratory for Electron Microscopy and 3DMM2O Cluster of Excellence (EXC 2082/1−390761711), Karlsruhe Institute of Technology (KIT), Karlsruhe 76131, Germany; Material Research Center for Energy Systems (MZE), Karlsruhe Institute of Technology (KIT), Karlsruhe 76131, Germany*

Erich Müller − *Laboratory for Electron Microscopy, Karlsruhe Institute of Technology (KIT), Karlsruhe 76131, Germany; Material Research Center for Energy Systems (MZE), Karlsruhe Institute of Technology (KIT), Karlsruhe 76131, Germany*

Christian Sprau − *Light Technology Institute, Karlsruhe Institute of Technology (KIT), Karlsruhe 76131, Germany; Material Research Center for Energy Systems (MZE), Karlsruhe Institute of Technology (KIT), Karlsruhe 76131, Germany*

Alexander Colsmann − *Light Technology Institute, Karlsruhe Institute of Technology (KIT), Karlsruhe 76131, Germany; Material Research Center for Energy Systems (MZE), Karlsruhe Institute of Technology (KIT), Karlsruhe 76131, Germany;* orcid.org/0000 0001 9221 9357

Author Contributions

D.G., E.M., and Y.L. conceived the project and experiment. Y.L. carried out the experiments and analysis. M.C. and Y.L. conducted the FIB SEM tomography and data analysis. C.S. and A.C. designed and fabricated the BHJ layers. The manuscript was written by Y.L. and D.G. All authors discussed the data and read and approved the final manuscript.

Notes

The authors declare no competing financial interest.

ACKNOWLEDGMENTS

M.C. and D.G. acknowledge funding by the Deutsche Forschungsgemeinschaft (DFG, German Research Foundation) under Germany's Excellence Strategy−2082/1−390761711 and thank the Carl Zeiss Foundation for the financial support. Y.L. acknowledges the support of the Alexander von Humboldt Foundation. C.S. and A.C. acknowledge the support by the Helmholtz Program "Materials and Technologies for the Energy Transition". We also thank Felix Manger (Light Technology Institute, Karlsruhe Institute of Technology) for providing P3HT and $PC_{61}BM$ layers.

REFERENCES

(1) Michler, G. H. *Electron Microscopy of Polymers*; Springer: Berlin, 2008.

(2) Bozzola, J. J.; Russell, L. D. *Electron Microscopy: Principles and Techniques for Biologists*; Jones and Bartlett: Boston, 1999.

(3) Sawyer, L.; Grubb, D. T.; Meyers, G. F. *Polymer Microscopy*; Springer: New York, 2008.

(4) Liu, F.; Gu, Y.; Jung, J. W.; Jo, W. H.; Russell, T. P. On the Morphology of Polymer Based Photovoltaics. *J. Polym. Sci., Part B: Polym. Phys.* **2012**, *50*, 1018−1044.

(5) Hoppe, H.; Sariciftci, N. S. Morphology of Polymer/Fullerene Bulk Heterojunction Solar Cells. *J. Mater. Chem.* **2006**, *16*, 45−61.

(6) van Bavel, S. S.; Sourty, E.; de With, G.; Loos, J. Three Dimensional Nanoscale Organization of Bulk Heterojunction Polymer Solar Cells. *Nano Lett.* **2009**, *9*, 507−513.

(7) Drummy, L. F.; Davis, R. J.; Moore, D. L.; Durstock, M.; Vaia, R. A.; Hsu, J. W. P. Molecular Scale and Nanoscale Morphology of P3HT: PCBM Bulk Heterojunctions: Energy Filtered TEM and Low Dose HREM. *Chem. Mater.* **2011**, *23*, 907−912.

(8) Moon, J. S.; Takacs, C. J.; Sun, Y.; Heeger, A. J. Spontaneous Formation of Bulk Heterojunction Nanostructures: Multiple Routes to Equivalent Morphologies. *Nano Lett.* **2011**, *11*, 1036−1039.

(9) Pfannmöller, M.; Flügge, H.; Benner, G.; Wacker, I.; Sommer, C.; Hanselmann, M.; Schmale, S.; Schmidt, H.; Hamprecht, F. A.; Rabe, T.; Kowalsky, W. Visualizing a Homogeneous Blend in Bulk Heterojunction Polymer Solar Cells by Analytical Electron Microscopy. *Nano Lett.* **2011**, *11*, 3099−3107.

(10) Wen, J.; Miller, D. J.; Chen, W.; Xu, T.; Yu, L.; Darling, S. B.; Zaluzec, N. J. Visualization of Hierarchical Nanodomains in Polymer/Fullerene Bulk Heterojunction Solar Cells. *Microsc. Microanal.* **2014**, *20*, 1507−1513.

(11) Rechberger, S.; Gasparini, N.; Singh, R.; Kim, M.; Chochos, C. L.; Gregoriou, V. G.; Cho, K.; Brabec, C. J.; Ameri, T.; Spiecker, E.

Unraveling the Complex Nanomorphology of Ternary Organic Solar Cells with Multimodal Analytical Transmission Electron Microscopy. *Solar RRL* **2020**, *4*, 2000114.
(12) Masters, R. C.; Pearson, A. J.; Glen, T. S.; Sasam, F. C.; Li, L.; Dapor, M.; Donald, A. M.; Lidzey, D. G.; Rodenburg, C. Sub Nanometre Resolution Imaging of Polymer−Fullerene Photovoltaic Blends Using Energy Filtered Scanning Electron Microscopy. *Nat. Commun.* **2015**, *6*, 6928.
(13) Klein, M. F. G.; Pfaff, M.; Müller, E.; Czolk, J.; Reinhard, M.; Valouch, S.; Lemmer, U.; Colsmann, A.; Gerthsen, D. Poly (3 Hexylselenophene) Solar Cells: Correlating the Optoelectronic Device Performance and Nanomorphology Imaged by Low Energy Scanning Transmission Electron Microscopy. *J. Polym. Sci., Part B: Polym. Phys.* **2012**, *50*, 198−206.
(14) Li, Y.; Müller, E.; Sprau, C.; Colsmann, A.; Gerthsen, D. Imaging of Polymer: Fullerene Bulk Heterojunctions in a Scanning Electron Microscope: Methodology Aspects and Nanomorphology by Correla tive SEM and STEM. *Adv. Struct. Chem. Imaging* **2020**, *6*, 1−12.
(15) Mu, X.; Mazilkin, A.; Sprau, C.; Colsmann, A.; Kübel, C. Mapping Structure and Morphology of Amorphous Organic Thin Films by 4D STEM Pair Distribution Function Analysis. *Microscopy* **2019**, *68*, 301−309.
(16) van Bavel, S. S.; Loos, J. Volume Organization of Polymer and Hybrid Solar Cells as Revealed by Electron Tomography. *Adv. Funct. Mater.* **2010**, *20*, 3217−3234.
(17) Jin, S. M.; Nam, J.; Song, C. E.; Chung, H.; Kim, B.; Lee, E. The 3D Morphological Stability of P3HT Nanowire Based Bulk Hetero junction Thin Films against Light Irradiation Quantitatively Resolved by TEM Tomography. *J. Mater. Chem. A* **2019**, *7*, 2027−2033.
(18) Jung, H.; Jung, A. R.; Jin, S. M.; Kim, S.; Heo, H.; Nguyen, H. V. T.; Kim, M. J.; Ahn, P.; Kim, M. H.; Lee, Y.; Lee, K. K.; Cho, J. H.; Lee, E.; Kim, B. S. Influence of 3D Morphology on the Performance of All Polymer Solar Cells Processed Using Environmentally Benign Nonhalogenated Solvents. *Nano Energy* **2020**, *77*, 105106.
(19) Levitsky, A.; Matrone, G. M.; Khirbat, A.; Bargigia, I.; Chu, X.; Nahor, O.; Segal Peretz, T.; Moulé, A. J.; Richter, L. J.; Silva, C.; Stingelin, N.; Frey, G. L. Toward Fast Screening of Organic Solar Cell Blends. *Adv. Sci.* **2020**, *7*, 2000960.
(20) Wirix, M. J.; Bomans, P. H.; Hendrix, M. M.; Friedrich, H.; Sommerdijk, N. A.; de With, G. Visualizing Order in Dispersions and Solid State Morphology with Cryo TEM and Electron Tomography: P3HT: PCBM Organic Solar Cells. *J. Mater. Chem. A* **2015**, *3*, 5031−5040.
(21) Roehling, J. D.; Batenburg, K. J.; Swain, F. B.; Moulé, A. J.; Arslan, I. Three Dimensional Concentration Mapping of Organic Blends. *Adv. Funct. Mater.* **2013**, *23*, 2115−2122.
(22) Roehling, J. D.; Baran, D.; Sit, J.; Kassar, T.; Ameri, T.; Unruh, T.; Brabec, C. J.; Moulé, A. J. Nanoscale Morphology of PTB7 Based Organic Photovoltaics as a Function of Fullerene Size. *Sci. Rep.* **2016**, *6*, 30915.
(23) Heiber, M. C.; Herzing, A. A.; Richter, L. J.; DeLongchamp, D. M. Charge Transport and Mobility Relaxation in Organic Bulk Heterojunction Morphologies Derived from Electron Tomography Measurements. *J. Mater. Chem. C* **2020**, *8*, 15339−15350.
(24) Pfannmoller, M.; Heidari, H.; Nanson, L.; Lozman, O. R.; Chrapa, M.; Offermans, T.; Nisato, G.; Bals, S. Quantitative Tomography of Organic Photovoltaic Blends at the Nanoscale. *Nano Lett.* **2015**, *15*, 6634−6642.
(25) Herzing, A. A.; Richter, L. J.; Anderson, I. M. 3D Nanoscale Characterization of Thin Film Organic Photovoltaic Device Structures Via Spectroscopic Contrast in the TEM 1. *J. Phys. Chem. C* **2010**, *114*, 17501−17508.
(26) Sprau, C.; Kattenbusch, J.; Li, Y. H.; Müller, E.; Gerthsen, D.; Berger, R.; Michels, J. J.; Colsmann, A. Revisiting Solvent Additives for the Fabrication of Polymer:Fullerene Solar Cells: Exploring a Series of Benzaldehydes. *Sol. RRL* **2021**, *5*, 2100238.
(27) Chen, D.; Liu, F.; Wang, C.; Nakahara, A.; Russell, T. P. Bulk Heterojunction Photovoltaic Active Layers Via Bilayer Interdiffusion. *Nano Lett.* **2011**, *11*, 2071−2078.
(28) Wang, D.; Nakajima, K.; Liu, F.; Shi, S.; Russell, T. P. Nanomechanical Imaging of the Diffusion of Fullerene into Conjugated Polymer. *ACS Nano* **2017**, *11*, 8660−8667.
(29) Treat, N. D.; Brady, M. A.; Smith, G.; Toney, M. F.; Kramer, E. J.; Hawker, C. J.; Chabinyc, M. L. Interdiffusion of PCBM and P3HT Reveals Miscibility in a Photovoltaically Active Blend. *Adv. Energy Mater.* **2011**, *1*, 82−89.
(30) Liu, F.; Zhao, W.; Tumbleston, J. R.; Wang, C.; Gu, Y.; Wang, D.; Briseno, A. L.; Ade, H.; Russell, T. P. Understanding the Morphology of PTB7: PCBM Blends in Organic Photovoltaics. *Adv. Energy Mater.* **2014**, *4*, 1301377.
(31) Lachkar, A.; Selmani, A.; Sacher, E.; Leclerc, M.; Mokhliss, R. Metallization of Polythiophenes I. Interaction of Vapor Deposited Cu, Ag and Au with Poly (3 Hexylthiophene)(P3HT). *Synth. Met.* **1994**, *66*, 209−215.
(32) Elfeninat, F.; Fredriksson, C.; Sacher, E.; Selmani, A. A Theoretical Investigation of the Interactions between Thiophene and Vanadium, Chromium, Copper, and Gold. *J. Chem. Phys.* **1995**, *102*, 6153−6158.
(33) Voreades, D. Secondary Electron Emission from Thin Carbon Films. *Surf. Sci.* **1976**, *60*, 325−348.
(34) Arganda Carreras, I.; Kaynig, V.; Rueden, C.; Eliceiri, K. W.; Schindelin, J.; Cardona, A.; Sebastian Seung, H. Trainable Weka Segmentation: A Machine Learning Tool for Microscopy Pixel Classification. *Bioinformatics* **2017**, *33*, 2424−2426.
(35) Hayat, M. E. *Fixation for Electron Microscopy*; Academic Press: New York, 1981.
(36) Cliff, G.; Lorimer, G. W. The Quantitative Analysis of Thin Specimens. *J. Microsc.* **1975**, *103*, 203−207.